Self-Affine Surfaces of Polymer Brushes

ARTICLE *in* MACROMOLECULES · JULY 2007

Impact Factor: 5.8 · DOI: 10.1021/ma0708794

Self-Affine Surfaces of Polymer Brushes

Bulent Akgun,[†] Dong Ryeol Lee,*[,‡,⊥] Hyeonjae Kim,[†] Haining Zhang,[§] Oswald Prucker,[§] Jin Wang,[‡] Jürgen Rühe,[§] and Mark D. Foster*[,†]

Maurice Morton Institute of Polymer Science, University of Akron, Akron, Ohio 44325; X-ray Science Division, Argonne National Laboratory, Argonne, Illinois 60439; and Department for Microsystems Engineering (IMTEK), University of Freiburg, Freiburg, Germany

Received April 14, 2007; Revised Manuscript Received June 18, 2007

ABSTRACT: The diffuse X-ray scattering from the surface morphology of polystyrene (PS) and poly(*n*-butyl acrylate) (P*n*BA) brushes synthesized by conventional free radical polymerization is found to be well described by a model of a surface with self-affine roughness. To date, such models have only been used with solid surfaces. The signature behavior of capillary waves is not observed. Data collected from transverse scans at multiple values of the out-of-plane momentum transfer q_z can be fit simultaneously using a single set of the roughness parameters: the root-mean-square roughness, σ, the lateral correlation length, ξ, and the roughness exponent, h. The surfaces of the P*n*BA brushes are the same at temperatures 75 and 130 °C above the glass transition temperature, T_g, of P*n*BA in the bulk. In contrast, the correlation lengths of the surface structures of PS brushes annealed at 140 °C are lower than those of the "as-deposited" brushes, and the roughnesses increase with annealing. The lateral correlation length, ξ, of the annealed PS brushes varies with brush thickness, d, as $\xi \sim d^{0.75}$, which matches the power law dependence expected for the variation of the predominant wavelength of surface fluctuations with brush thickness for a melt brush in the limit of high surface tension. The roughness of the annealed PS brushes increases as a power law of d, with an exponent similar to those characterizing "kinetic roughening" in plasma deposited polymer films.

Introduction

The structure and dynamics of the surface of a thin polymer film affect wetting of the film, adhesion to it, and friction against it. Thin films consisting of "polymer brushes" have recently attracted interest because they are particularly resistant to damage by solvents or high temperature. Polymer brushes are formed by tethering one end of each chain in an ensemble of chains to a surface sufficiently close together that the chains must stretch appreciably away from the Gaussian coil configurations preferred in a melt of untethered chains.[1] The stretching of the chains can cause the film to have physical properties different from those of corresponding polymer films in which the chains are not tethered.

The surfaces of low molecular weight liquids have microroughnesses dictated by the presence of thermally stimulated capillary waves. That is, the capillary waves are a dynamical phenomenon, but their presence is evident in, for example, results from static scattering experiments, which capture only a snapshot or time-averaged characterization of the surface structure. The morphology and dynamics of the surfaces of low molecular weight liquid films,[2−6] spun-cast polymer films,[7−9] and free-standing polymer films[10−12] have been extensively studied using X-ray diffuse scattering and reflectivity. The X-ray diffuse scattering from the surface of a typical liquid is consistent with the standard theory of thermally stimulated capillary waves.[3,6] One diffuse scattering experiment appropriate for observing signature behavior of capillary waves is the "transverse scan", which can be briefly described using the schematic

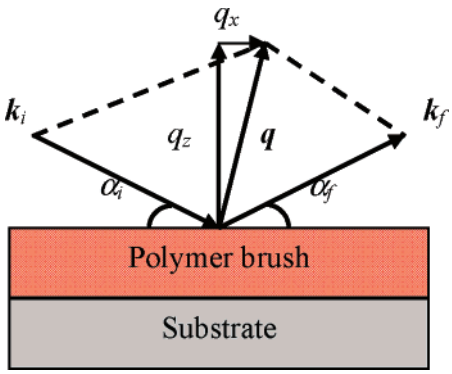

Figure 1. Scattering geometry of the X-ray experiment is shown with incident and scattered wave vectors k_i and k_f and the incidence and exit angles α_i and α_f, respectively. q is the scattering vector with perpendicular component q_z and in-plane component q_x. Specular scattering corresponds to $\alpha_i = \alpha_f$. Otherwise, the scattering is called off-specular diffuse scattering.

of the scattering geometry in Figure 1. The in-plane component of the scattering vector **q** (q_x) is varied while the component perpendicular to the surface is kept constant. If the scattering is measured using a slit-collimated beam with integration in the q_y direction, the diffuse scattering should vary[13] as $q_x^{\eta-1}$ with the value of the exponent varying with q_z, the surface tension of the fluid, γ, and temperature, T, as $\eta = Bq_z^2/2$ and $B = k_BT/\gamma$ with k_B being the Boltzmann constant. So the slope of a log−log plot of intensity vs q_x is expected to decrease with increasing q_z with the slope remaining close to, but larger than, −1. For thin films, suppression of the capillary waves occurs for sufficiently large values of wavelength, that is for values of wavevector, q_x, below a lower wavevector cutoff, $q_{l,c}$, due to interactions between the substrate and the surface.

Wang et al.[8] studied the surface structure of quenched, spun-cast films of untethered polystyrene (PS) by diffuse X-ray scattering. They reported a suppression of surface fluctuations

* Corresponding authors. E-mail: mfoster@uakron.edu, drlee@postech.ac.kr.
† University of Akron.
‡ Argonne National Laboratory.
§ Institute for Microsystem Technology.
⊥ Present address: Pohang Accelerator Laboratory, Pohang University of Science and Technology, Korea.

10.1021/ma0708794 CCC: $37.00
Published on Web 07/28/2007

for values of q_x below a lower wavevector cutoff, $q_{l,c}$, but the data could not be interpreted fully using capillary wave calculations assuming attractive van der Waals interactions between the substrate and the film. It has been demonstrated with various sorts of measurements that thin films of untethered chains on substrates are in a strongly confined state due to interactions with the substrate surface.[14]

Lurio et al.[15] used off-specular measurements placed on an absolute intensity basis to study the surface tension and surface roughness of supported films of PS (M = 123K) of various thicknesses and at various temperatures *without quenching*. They found that capillary wave theory could explain the off-specular scattering at temperatures above the glass transition temperature, T_g, over most of the range of length scales probed, but the total roughness exceeded that expected from capillary wave theory, indicating the presence of excess roughness at length scales less than 2 nm.

Results of static off-specular scattering experiments published recently by Seo and co-workers[16] demonstrate that the surface fluctuation behavior of films of untethered polymer chains cannot be understood without accounting explicitly for chain length. For lengths, N, which are less than or close to N_e, the entanglement length, simple liquidlike scaling is observed. When N becomes much larger than N_e, a different behavior is found which the authors identify as "brushlike", in the sense of the brush structure introduced by Guiselin.[17] Guiselin considered a layer of polymer chains adsorbed to a surface from a melt or concentrated solution. These authors find that for $d/R_g < 2$ there appears to be additional suppression of surface modes. Li et al.[18] provided additional evidence that the chains closest to the substrate adsorb to the substrate in such a way that the viscosity of a film thinner than $2R_g$ is very large. The results of this pinning effect can be propagated to the surface of films thicker than $2R_g$ if other chains become entangled with the pinned layer.

Polymer brushes in which each chain is covalently tethered to the substrate by one end represent an interesting limit to the general case of films in which the effects of interactions with the substrate can propagate through the film. Each chain feels a strong interaction with the substrate, but additionally there is strong repulsion between pairs of chains once the grafting density is high enough. The chain conformation is highly distorted from that of random coils. Although the chemistry,[19−24] composition profile,[25−29] and collective dynamics[30−33] of "wet" (in solvent) homopolymer brushes have been investigated, the surface structure and dynamics of neat brushes at temperatures above the bulk T_g of untethered chains (and therefore in a putative "melt" state) have been little studied and are not clearly understood. Fredrickson and co-workers[34] argued that the long wavelength fluctuations should be highly suppressed on the surface of a polymer brush due to the entropic penalty chains have to pay to create these undulations. They also argued that the shortest wavelength fluctuations should be suppressed due to the action of surface tension. They calculated that the structure factor has a broad peak at a wavevector q^*, corresponding to a dominant wavelength for the thermally excited surface mode of a molten polymer brush. This dominant wavelength should be on the order of equilibrium brush thickness. Later, Xi and Milner[35] reached the same conclusion though they started with different assumptions about the locations of the free ends of the tethered chains.

Akgun et al.[36] studied the static structure of brushes of diblock copolymer chains with narrow polydispersity and found for low molecular weight brushes with thickness $>4R_g$ that the surface roughness was correlated with that of the very smooth silicon substrate. Thus, interface correlation was found for a thickness more than 3 times that for which correlation was observed for small molecule liquid films.[4] This was indirect evidence that fluctuations at the surface of the brush were suppressed. The study of surface structure of homopolymer brushes made by free radical polymerization with diffuse X-ray scattering was first reported by Foster et al. in an earlier publication.[37] It was reported that the surface structure varied systematically with brush thickness. In a qualitative analysis, the shapes of transverse scans from the brushes were attributed to the presence of surface fluctuations at small wavelengths and suppression of fluctuations at large wavelengths. However, the scattering curves were not fit with detailed models, and some of the observed behavior was not consistent with surface structures dictated by the presence and suppression of surface fluctuations over particular ranges of wavelength. Thus, while it could still be true that surface fluctuations were suppressed on those samples, the aspect of the brush surfaces primarily evidenced by the X-ray scattering was something other than that of surface wave suppression.

In this paper we offer a more detailed and consistent analysis of those data from quenched, polydisperse PS and molten polydisperse poly(*n*-butyl acrylate) (P*n*BA) homopolymer brushes having molecular weights much higher than those studied with the atom transfer radical polymerization (ATRP) brushes. We find that both the diffuse X-ray data and complementary atomic force microscopy data from the surface morphologies of the free-radical-polymerized PS brushes annealed above T_g and then quenched may be well described by a model of self-affine (self-similar) roughness that to date has only been used to describe isotropic solid surfaces. In the wavelength range studied with X-ray scattering, the model based on a self-affine surface is much better suited to simulate the diffuse scattering data. We underscore that the self-affine model quantitatively and self-consistently describes all the data available. The surfaces of the P*n*BA brushes are likewise self-affine.

Experimental Section

PS and P*n*BA brushes were synthesized using surface-initiated conventional free radical polymerization techniques as described in the literature.[19−21] There were two sets of samples. In the first set, brush film thickness was increased by increasing grafting density at a fixed molecular weight. This series of samples will be identified by the label "GDV" ("grafting density varied"). Grafting density is a function of initiator decomposition rate, initiator efficiency, reaction temperature, and reaction time. The latter parameter was used to adjust the conversion of the initiator and thereby the number of polymer chains generated at the surface. To make molecular weights the same throughout this series of samples, the concentration of styrene monomer was kept constant (50 vol %). Since the values of all other polymerization parameters except reaction time were constant, grafting density was determined by reaction time.

In the second series, brush film thickness was increased by increasing the molecular weight of the surface-attached polymers at a fixed grafting density. This series of samples will be denoted by "MWV" ("molecular weight varied"). For this set, molecular weight of the brush chains is a function of monomer concentration, reaction time, and reaction temperature. To make grafting densities the same throughout this series of samples, each polymerization was carried out for 5 h. Because all polymerization parameters except monomer concentration were held fixed, molecular weight was determined by monomer concentration.

The thicknesses of the P*n*BA brush films were controlled by varying reaction time using bulk monomer in order to vary grafting density, except for the thinnest brush. The thinnest one was prepared with a 50 vol % solution. A summary of the estimated molecular

Table 1. Summary of Characteristics of Brush Samples

sample series	d^a (nm)	σ^b (nm)	grafting density (chains/nm^2)	$M_n{}^c$ (10^5 g/mol)	spacing between attachment points (nm)	d/R_g	I^e
PS GDV	9	0.5	0.025	6.5	6.3	0.4	1500
	43	1.4	0.056	6.5	4.2	2.0	65
	62	1	0.077	6.5	3.6	2.9	24
	96	1.6	0.097	6.5	3.2	4.5	10
	136	1.2	0.14	6.5	2.7	6.3	3
	251	–	0.2	8.1	2.2	10.4	0.9
PS MWV	10	0.5	0.066	4.2	3.9	0.6	210
	23	0.7		4.8		1.2	87
	33	0.8		5.3		1.7	61
	47	0.9		5.9		2.3	42
	54	1		6.5		2.5	37
	83	1.3		8.1		3.4	24
P*n*BA	13	1.2	0.024	25[d]	6.4	0.3	750
	25	2.2	0.024		6.4	0.7	390
	89		0.036		5.3	2.3	55
	284		0.054		4.3	7.4	7
	330		0.078		3.6	8.6	3

[a] Measured by either XR or ellipsometry. Uncertainty in d measured by XR is $<\pm 2$ Å. [b] Values of roughness, σ, are shown only for the samples measured by XR. Uncertainty of σ inferred from the fitting process is about 15−20%. [c] As determined by gel permeation chromatography (GPC system from Agilent with columns from PSS, Mainz, Germany) calibrated using narrow molecular weight distribution PS standards purchased from PSS (Mainz, Germany).[d] The molecular weight of each P*n*BA brush was estimated from the known kinetics of the polymerization process using published values[19−21] for the graft density of the initiator and all kinetic constants. These values allow for an estimation of the graft density of the polymers which together with the layer thickness and the materials density (taken as 1 g mL^{-1}) allows for the calculation of the number-averaged molecular weight. The error of this calculation stems from variables during the polymerization process and may be estimated to be of the order of 30%. [e] Dimensionless surface tension calculated using eq 3.

weights, grafting densities, sample thicknesses, and root-mean-square roughness values measured by X-ray reflectivity (XR) is given in Table 1.

The PS brushes were measured before and after annealing. Annealing was performed in a high-vacuum oven (1.04×10^{-4} Pa). Annealing times were constrained by the susceptibility to thermal degradation of the chain linkages to the substrate. Using experience in Rühe's group with various thermal treatments as a guide, an annealing time of 20 min was chosen to provide substantial opportunity for relaxation of the surface without danger of cleaving chains from the surface. Because of limitations in the heating and cooling rates of the heating device in the oven, in addition to the 20 min at 140 °C, the samples spent about 25 min at temperatures above T_g of untethered chains as they were first heated to 140 °C and then while they were cooled after a residence time at 140 °C. When a sample's temperature dropped below T_g of the untethered chains, the sample was taken out of the oven and put on a large, cold aluminum plate to cool rapidly. This annealing time of 20 min is not sufficient for center-of-mass diffusion of untethered chains of comparable molecular weight over distances comparable to R_g, but such large scale motion is not needed to relax the surface structure. Untethered P*n*BA chains have a bulk $T_g \approx -54$ °C,[38] and bulk P*n*BA is rubbery at room temperature, so the P*n*BA brushes were not annealed.

In specular X-ray reflectivity the incident angle is equal to the exit angle ($\alpha_i = \alpha_f$). The scattering vector, **q**, lies perpendicular to the surface, and the experiment is sensitive to the structure of thin films in the direction normal to the surface. With the normal direction denoted as z, **q** has only a q_z component, as is shown in Figure 1. In diffuse X-ray scattering, at least one in-plane component of **q** (q_x or q_y) is nonzero. This allows one to explicitly study lateral length scales of the surface structure. Since this is a static scattering experiment, it is actually the structure of the surface that is probed, and information about the surface dynamics is inferred from characteristics of the surface structure. In the case that the surface of the brush is vitrified before the measurement is made, a "snapshot" of the surface fluctuations is studied. If the surface is in the melt state during the measurement, information pertinent to a time average of the surface structure is collected.

Specular X-ray reflectivity and transverse diffuse scans were measured on the 1-BM beamline at the Advanced Photon Source in Argonne National Laboratory. The wavelength of 0.113 nm was chosen using a double-crystal monochromator, and the resolution Δq_x was 8×10^{-4} nm^{-1} at $q_z = 2$ nm^{-1}. The ratio of detector slit height (h_d) to the height of the incident beam (h_i) was 1.89. The samples were placed on a goniometer providing translations in x, y, and z and rotation in theta (incident angle). A NaI scintillation counter was used to collect the scattered intensity. Transverse diffuse scans were performed as step scans holding q_z constant at 1.5, 2, 3, or 3.5 nm^{-1}. The values of q_x used for the scans were optimized for each sample to provide approximately a logarithmic spacing of data points. Radiation damage was minimized by translating the samples perpendicular to the beam direction after each scan. A spot on a sample was typically exposed for 10−20 min, with longer exposures corresponding to cases in which the beam was attenuated for a substantial fraction of the total time. The flux of the unattenuated beam was about 2×10^{11} photons/(s cm^2).

The surface morphology of some samples was also checked with atomic force microscopy (AFM). AFM measurements were made in intermittent-contact (tapping) mode using a Veeco Dimension 3100 in a clean room with a silicon tip that had a spring constant of 40 N/m and resonant frequency of 170 kHz. Surface structure factors were calculated from the AFM images in order to compare to the scattering data.

Results and Discussion

The surface structure of the homopolymer brushes was studied to elucidate the effect of tethering on the surface dynamics and morphology. The effects of grafting density and molecular weight on the surface structure were also probed using the GDV and MWV samples. Figure 2 shows a typical plot of specular reflectivity for a 45 nm thick annealed PS brush sample. The reflectivity has been multiplied by $q_z{}^4$ to emphasize the fringes and to normalize for the trivial $q_z{}^{-4}$ dependence present for any interface for q_z markedly beyond the critical value. The solid curve is a fit obtained with the dispersion profile shown in the inset. We used the Parratt[39] recursive relation modified for rough interfaces and determined the best fitting parameters using a nonlinear least-squares fitting method. The dispersion, δ, is the real part of the X-ray refractive index and readily related to the electron density of a material. The model contains regions corresponding to the Si substrate, thin silicon oxide layer, and the PS brush film, with the mass density of the brush set to the nominal bulk value for PS ($\rho = 1.05$ g/cm^3). The thickness of the silicon oxide layer was consistent for all fits, and it was 1.3

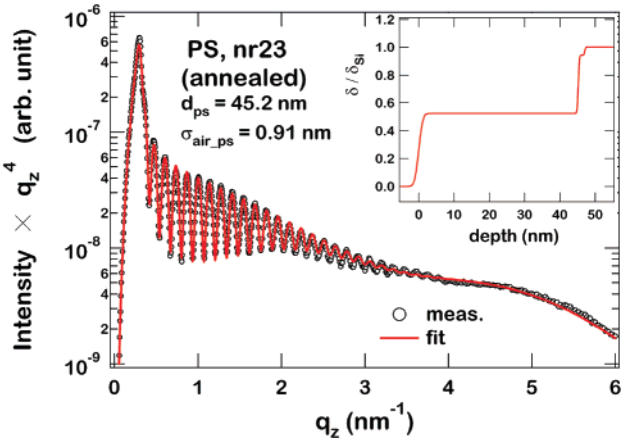

Figure 2. Specular reflectivity (circles) and best fit (solid curve) from a 45 nm thick annealed PS brush sample. Multiplying the scattering intensities by q_z^4 emphasizes the fringes and normalizes for the trivial q_z^{-4} dependence. Inset shows the profile of the dispersion, normalized by δ_{Si}, obtained for the model explained in the text.

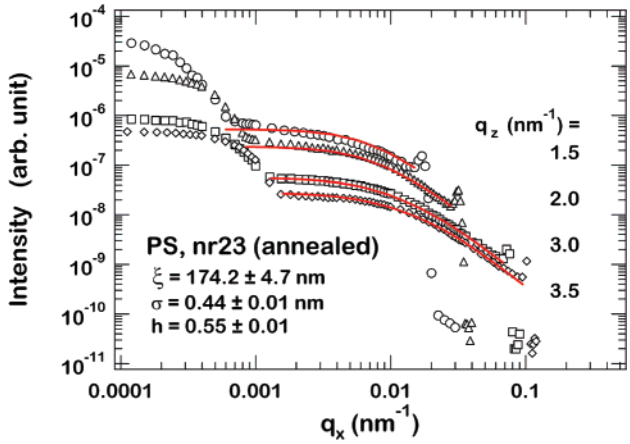

Figure 3. Transverse scans (circles) taken at $q_z$values of 1.5, 2, 3, and 3.5 nm^{-1} and the best fits from the self-affine model (solid curve) for the 45 nm thick annealed PS brush.

± 0.2 nm. The reflectivity data sets from the whole series of brush samples were successfully fit using the same sort of model.

While specular reflectivity gives an averaged picture of the surface morphology, more insight into the structure in the lateral direction is provided by analysis of the diffuse scattering data. First, an attempt was made to explain the transverse scan data using the standard capillary wave theory, but the value of the exponent for the scaling of the diffuse intensity with in-plane wavevector was not consistent with the capillary wave model. Supposing that there was surface morphology that was not due completely to capillary waves, the model was modified to include surface height fluctuations from both capillary waves and static variations in brush thickness. These might be due to, for example, lateral inhomogeneities in grafting density. This model also did not fit the observed transverse scan data. Finally, a model with self-affine roughness was found to represent the data quite nicely, even though this characteristic roughness has to date been associated with isotropic solid surfaces. The height−height correlation function, $C(x,y)$, for a self-affine surface with the lateral correlation length, ξ, proposed by Sinha and co-workers,[40] is given as

$$C(x,y) = C(R) = \sigma^2 e^{-(R/\xi)^{2h}} \quad (1)$$

where σ is the root-mean-square roughness and h is the roughness exponent. Small values of h correspond to jagged surfaces, while values of h approaching 1 model smooth surfaces. The transverse scan data with different q_z values were simultaneously fitted using a set of fitting parameters, σ, ξ, and h. Figure 3 shows the experimental transverse scan data taken for a 45 nm thick annealed PS brush at four different q_z values together with the best fits obtained using the self-affine model. The Gaussian line shape of the data at the lowest q_x values is a portion of the profile of the specular beam and was not included in the fits. Likewise, the Yoneda[41] peaks observed at the large q_x end of the diffuse scattering are not modeled explicitly here. The quality of the fits is outstanding. The best fit gives $\xi = 174.2 \pm 4.7$ nm, $\sigma = 0.44 \pm 0.01$ nm, and $h = 0.55 \pm 0.01$.

For some samples, comparison was made between the diffuse scattering data and AFM images of the surface structure. To directly compare the AFM data with X-ray diffuse scattering intensities, $\exp[iq_z h_{AFM}(x,y)]$ and the square of its two-dimensional Fourier transformation were calculated from the measured surface height profile $h_{AFM}(x,y)$. Accounting for the fact that the X-ray experiment integrates over q_y, the function $S_{AFM}(q_x,q_z)$ corresponding to the X-ray scattering function $S(q_x,q_z)$ is

$$S_{AFM}(q_x,q_z) = \frac{1}{q_z^2}\int dq_y \left| \int dx\, dy\, e^{iq_z h_{AFM}(x,y)} e^{i(q_x x + q_y y)} \right|^2 \quad (2)$$

1 μm × 1 μm and 10 μm × 10 μm AFM images for the 31 nm thick annealed PS sample are shown in parts a and b of Figure 4, respectively. Each image provides a portion of the function $S_{AFM}(q_x,q_z)$ over a different range of q. The functions deduced from these images are compared with the X-ray diffuse scattering data in Figure 4c. The agreement between the AFM data and the X-ray data is excellent.

In Figure 5, transverse diffuse scans are shown along with the best fits using the self-affine model for the 13 nm thick P*n*BA brush at room temperature and at 80 °C. The P*n*BA brushes were measured at 80 °C to ensure that no residual solvent was present in the brush. No difference in the thicknesses measured at room temperature and 80 °C was observed, suggesting that there was no residual solvent. The diffuse scattering at 80 °C could be fit using model parameter values that were indistinguishable from those used to fit the room temperature data. If the diffuse scattering were dictated by dynamic (capillary wave) behavior of the surface, some change in the scattering with temperature should have been observed. A possible explanation is that the surface dynamics are suppressed at room temperature on the length scales probed here (8000−60 nm) and still suppressed at 80 °C, which would be remarkable, since the bulk T_g of untethered chains is −54 °C.[38]

Fits with the self-affine model to the diffuse data at $q_z = 3$ nm^{-1} are shown in Figure 6 for both the unannealed and annealed PS brushes of the "MWV" and "GDV" series, except for the thinnest sample of the "GDV" series. The thicknesses obtained independently from XR are shown next to the curves. The thinnest brush of the "GDV" series has diffuse scattering that is nearly describable with a single power law (not shown here). One might imagine that this shape could be due to the dominant role of van der Waals interactions between the substrate and polymer film in such a thin sample. However, comparison of the data from this sample with that from the sample of similar thickness in the "MWV" series does not support this argument. The only difference between these two samples is the grafting density of the polymer chains. Although

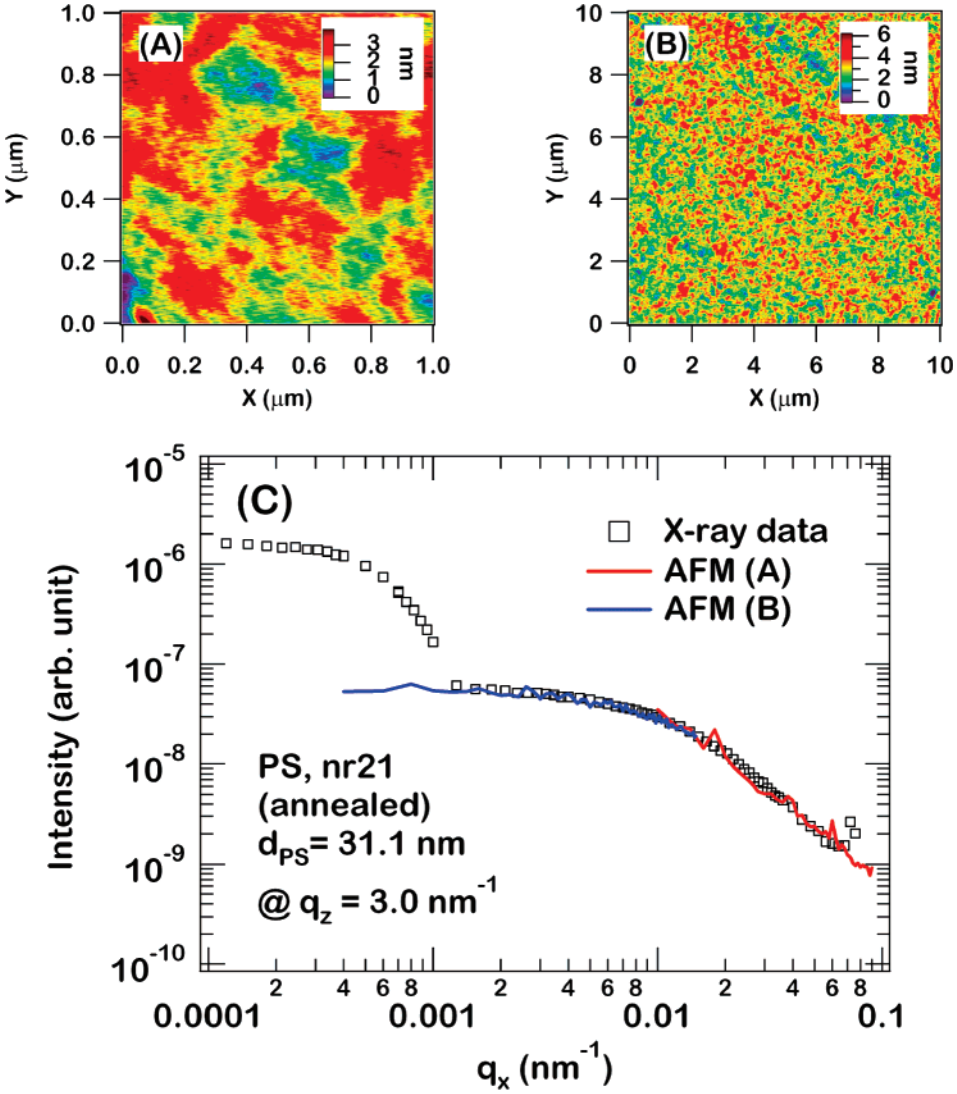

Figure 4. AFM images of (a) 1 μm × 1 μm and (b) 10 μm × 10 μm areas and (c) comparison of $S_{AFM}(q_x,q_z)$ calculated using eq 2 from these two images with the X-ray diffuse scattering intensities for a 31 nm thick PS brush.

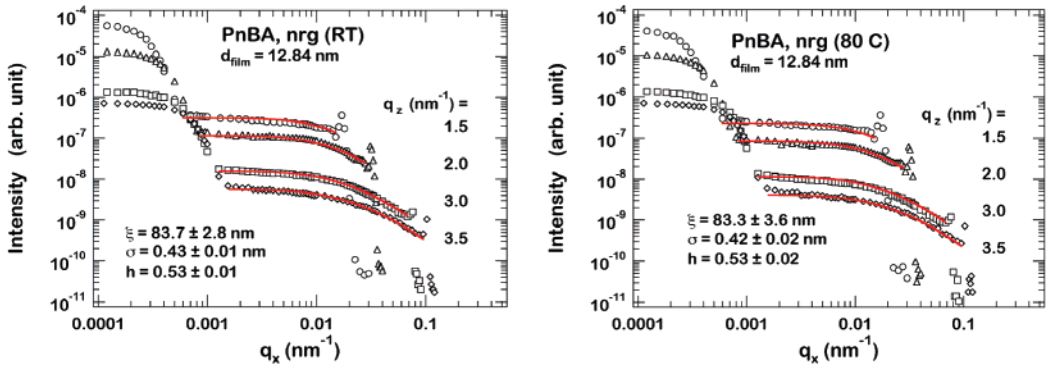

Figure 5. Transverse scans (circles) taken at q_z values of 1.5, 2, 3, and 3.5 nm^{-1} and the best fits from self-affine model (solid curve) for the 13 nm thick P*n*BA brush at room temperature (RT) and at 80 °C.

the thinnest brush of the "MWV" series has a higher grafting density than does the thinnest brush of the "GDV" series, the spacing between the anchoring points on the substrate is less than R_g of the chains for both. Thus, both films are in the brush regime. The observed behavior can be neither a result solely of grafting density difference nor completely a result of differences in van der Waals interactions.

Simultaneous fitting of all reflectivity profiles for the annealed and unannealed brush films demonstrates that the thickness generally decreases with annealing. (The apparent increase in thickness in the two thickest brushes is most likely due to fact that the thicknesses were not measured in precisely the same locations before and after annealing. Uniformity of thickness across the sample becomes increasingly difficult to maintain as thickness increases.) The lateral correlation length also decreases substantially (typically by at least 30%) after annealing. The correlation in the as-deposited sample is apparently dictated at least in part by details of the deposition history.

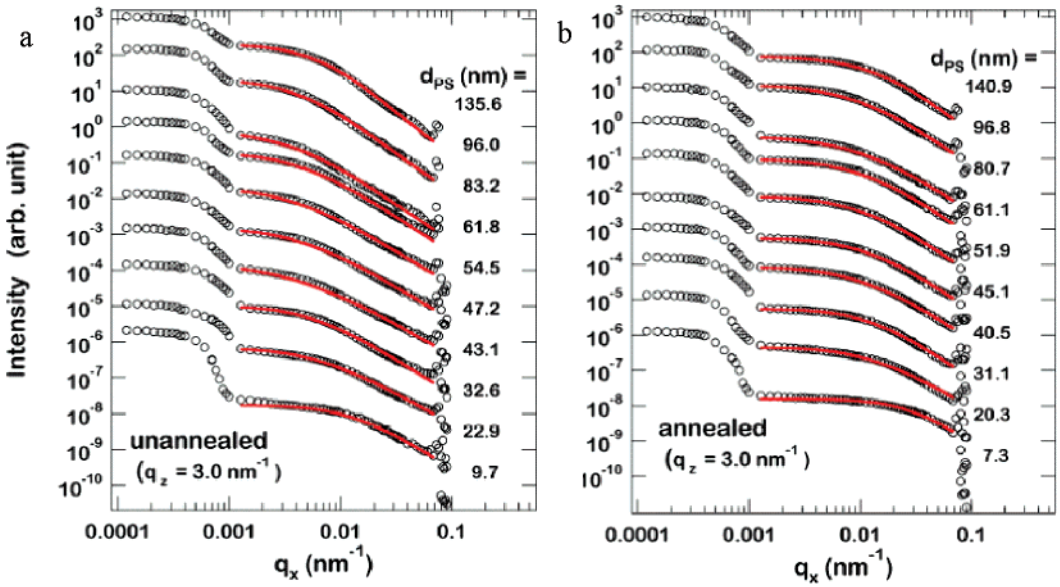

Figure 6. Transverse scans taken at $q_z = 3$ nm^{-1} for unannealed (a) and annealed (b) PS brushes with thicknesses varying from 7 to 140 nm with best fits using the self-affine model (solid curves). Each curve has been shifted vertically by an order of magnitude for clarity.

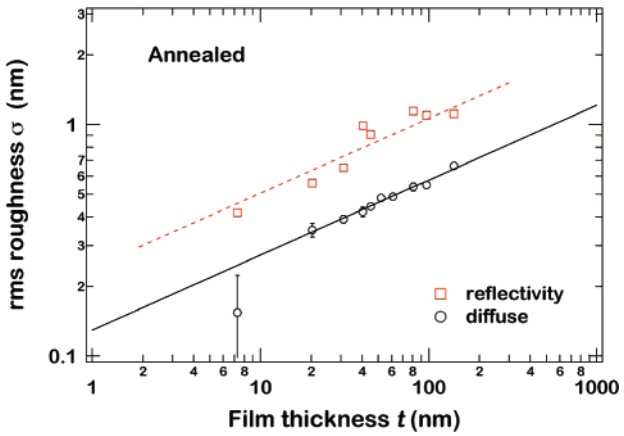

Figure 7. Rms roughnesses from reflectivity and off-specular diffuse scattering data fits as a function of film thickness for annealed PS brushes.

Lateral correlation in the structure caused by the deposition is relaxed by the increased mobility of the polymer chains at the surface during annealing.

The rms roughness values calculated from specular reflectivity and transverse diffuse scans for annealed PS brushes are plotted as a function of thickness in Figure 7, with the roughness value from reflectivity derived assuming that the effect of roughness can be captured by using a Gaussian interface profile. The magnitudes of rms roughnesses calculated from specular reflectivity and transverse scans differ because the two techniques are sensitive to different sorts of roughness. While the diffuse scattering probes only a laterally correlated roughness in the form of the height−height correlation function within the X-ray coherence length, the reflectivity measurement probes a laterally averaged roughness within the illuminated area. This averaged roughness can include various sorts of surface features such as sharp local bumps or steps, broadening of the interface due to interdiffusion, and surface bending. This difference between the roughnesses "seen" by reflectivity and diffuse scattering measurements has been used for distinguishing interdiffusion and interface roughness.[42,43] The maximum wavelength of roughness to which reflectivity is sensitive is dictated by the transverse coherence length of the beam, which is about 20 μm/sin(α_i). This is of the order of several 100 μm. The minimum roughness wavelength to which reflectivity is sensitive is very small, essentially molecular size. The diffuse scattering is sensitive to correlated roughness with wavelengths ranging from $2\pi/q_{x,max}$ to $2\pi/q_{x,min}$ (i.e., 80−5200 nm). Although the magnitudes are different, the variation of rms roughness with thickness can be described by a power law with an exponent of 0.32 ± 0.02 for both.

The self-affine model has been used to describe isotropic solid surfaces. The fact that our data are best modeled with the self-affine model suggests that the surfaces of both the PS and P*n*BA brushes have dynamics that are altered sufficiently as compared to those of untethered chains. In these "snapshots" of the structure remaining after quenching from above T_g the liquid character of the surface is not apparent. In the case of the P*n*BA brushes the state being studied should be one characteristic of a temperature far above the T_g of the corresponding untethered chains in bulk, which is −54 °C.[38] At room temperature, bulk P*n*BA behaves as a viscous liquid, but we conjecture that due to the confinement resulting from tethering, the surface of the P*n*BA brush has surface dynamics very different from those of viscous liquid of untethered chains. For the PS brushes the state probed by our experiment is less clearly defined, since the samples were cooled over 25 min from a temperature above room temperature. We discuss the PS brush *static* surface structure measured at room temperature as though it were the same as that found at the annealing temperature. This static structure at a temperature above the PS bulk T_g is strikingly different from that for comparably thick conventional films of untethered PS chains. Kim and co-workers[44−46] have shown, using X-ray photon correlation spectroscopy, that for films of *untethered* PS chains at $T \gg T_{g,bulk}$ the surface height−height correlations relax in a manner consistent with a model of overdamped capillary waves.[47] This difference in surface character of these two types of polymer films is a key focus of this contribution.

At present we do not have an explanation for why the surface should adopt the self-affine form, but the self-affine model has been used for parametrizing surface structures even when the self-affine form was not connected with a particular mechanism for the evolution of the surface.[48,49] However, it seems appropriate to make a comparison with the theory of Fredrickson et al.[34] in which they argue for the presence of a particular time-

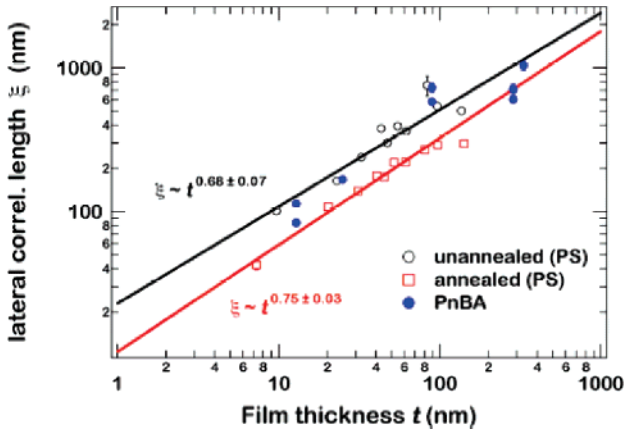

Figure 8. Variation of lateral correlation length with brush thicknesses for annealed PS (squares), unannealed PS (empty circles), and P*n*BA brushes (filled circles).

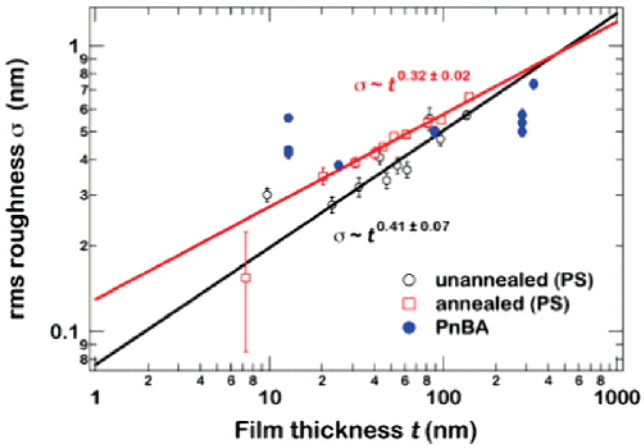

Figure 9. Dependence of the rms roughness calculated from the self-affine model on the brush thickness for unannealed PS, annealed PS and P*n*BA brushes.

averaged structure on the surface. They anticipate that the structure factor should have a broad peak at a wavevector q^* corresponding to the most probable thermally excited mode of a molten brush. This wavelength depends on the value of a dimensionless surface tension, Γ, defined as

$$\Gamma = \gamma/(\mu_0 d) \tag{3}$$

where γ is surface tension of the polymer, μ_0 is bulk shear modulus, and d is the equilibrium thickness of the polymer brush. The bulk shear modulus may be calculated as

$$\mu_0 = 3k_B T \frac{v\sigma^2}{b^2} \tag{4}$$

where v is the segment volume, σ is the grafting density, and b is the segment length. One obtains different expressions for q^* in two different limiting cases for Γ:

$$q^* d = 3^{1/3} \approx 1.44, \quad \Gamma \ll 1 \tag{5}$$

$$q^* d = (3/\Gamma)^{1/4}, \quad \Gamma \gg 1 \tag{6}$$

with (6) being the case for all but our thickest brush, as shown in Table 1. If one thinks of $1/q^*$ as a lateral correlation length for correlated roughness, one may replace $1/q^*$ with ξ in eq 6, and one obtains $\xi \sim d^{0.75}$ for the case of sufficiently high surface tension. The lateral correlation length, ξ, obtained from a fit to the diffuse scattering is shown as a function of brush film thickness for unannealed and annealed PS and P*n*BA brushes in Figure 8. The lateral correlation length varies with PS brush thickness, as $d^{0.75}$ after annealing, which is consistent with the expectations of Fredrickson et al.[34] For P*n*BA an exponent of 0.72 ± 0.01 is found.

The rms roughnesses obtained from fits to the diffuse scattering are plotted in Figure 9 as a function of thickness for all the samples studied. The amplitude of the roughness of an unannealed or as-deposited brush is dictated by the manner in which the brush "grew", the dynamics of the final brush in the presence of solvent, and the manner in which the brush collapsed as the solvent was removed very rapidly. The mechanism of brush polymerization dictates the polydispersity of the brush chains. For example, these free-radical-polymerized brushes have a larger chain length polydispersity than do brushes polymerized by ATRP.[50] The polydispersity, in turn, has implications for the brush dynamics in either the wet or dry states.[51] Before the collapse, the brush is swollen and has the dynamics of a wet brush that have been discussed by Fytas and co-workers.[30−33] As solvent is rapidly removed, the brush collapses and in the case of PS also vitrifies. At some point the structure present at the PS brush surface is trapped kinetically and cannot change further while the brush is dry and kept in a glassy state. The PS brush was annealed at a temperature substantially above the T_g of untethered PS chains of molecular weight comparable to that of the largest chains in the brush. A determination of T_g for a 42 nm thick PS brush using reflectivity measurements suggested that the T_g of these brushes are not altered strongly from the T_g of bulk PS. Therefore, it was supposed that this would bring the brush into a "melt" state in which it could manifest surface dynamics characteristic of a melt brush. When the sample was cooled, it was supposed that the structure trapped kinetically by cooling would be that characteristic of the surface at the glass transition temperature of the brush or perhaps some still higher temperature, but at least it would be characteristic of the melt state. Here we see a larger roughness after annealing.

For both as-deposited and annealed samples the variation in roughness with thickness can be described using a power law, which is what one expects in the case of kinetic roughening, where the evolution of the surface morphology of a thin film during growth can be classified by the scaling exponents for the rms surface roughness.[52] For kinetic roughening it is the competition between the processes of deposition and relaxation that dictate the roughness of the surface. For unannealed PS brushes $\sigma \sim d^{0.41\pm0.07}$, while for annealed PS brushes $\sigma \sim d^{0.32\pm0.02}$. The thickness dependence of the rms roughness is weaker for the P*n*BA brushes than for the PS brushes, and the trend is not so clear. The roughening of a film surface with increasing thickness for films that are deposited by "growing" on a substrate in some way has been studied for the metal and semiconductor thin films[53−59] and recently for plasma polymerized films.[60−62] Zhao et al.[61] found a power law dependence of roughness on thickness with an exponent of 0.25 ± 0.03 for linear poly(*p*-xylene) films grown by vapor deposition polymerization. Kardar and co-workers[63] considered the evolution of the profile of a growing interface for a vapor deposition process and predicted a value of the exponent of 1/3. For both plasma polymerization and "grafting from", a unit from which the film is built approaches the surface and then reacts with what is already on the surface. The roughening of the surface during the deposition depends on the deposition conditions and relaxation processes. However, in the polymerization used here there is no monomer deprivation at the growing chain ends, so

the deposition is not controlled by movement of the monomer to the growing ends. Thus, we come back to the idea that the dynamics of the assembly of polydisperse chains dictate the shape of the brush surface before collapse. When the solvent is removed, the PS chains are frozen at that moment, though there is a small amount of solvent trapped in the brush. It is very difficult to imagine the details of how the brush collapses. During annealing, we imagine the chains can move, but still their movement is limited since they are tethered to the substrate and they have to pay a huge entropic penalty to stretch.

Conclusion

Quantitative modeling of transverse X-ray scattering data from homopolymer brushes at temperatures far above the bulk T_g of the polymer or quenched rapidly from such a state reveals that the surfaces are self-affine. The observed scattering cannot be explained as resulting from capillary wave action in the range of length scale investigated, nor can it be rationalized as resulting from an island-like surface morphology. This admits the possibility that the dynamics of the brush surface are altered dramatically from those observed for comparably thick films of untethered chains. A variety of solid surfaces of various materials are known to produce scattering consistent with the self-affine surface model, but this is the first time such a surface has been observed for a material far above the bulk glass transition temperature. Variations in the brush surfaces with thickness followed the same trends whether the thickness was controlled by varying grafting density (GDV series) or molecular weight (MWV series), suggesting that once one is in the brush regime thickness becomes the overriding issue. The observation that the lateral correlation length varies as $\xi \sim d^{0.75}$ is reminiscent of the prediction of Fredrickson et al.[34] in the limit of large surface tension that the wavevector of the most probable fluctuation in the brush should scale as $1/q^* \sim d^{0.75}$. The roughnesses of the PS brushes appear to follow power laws in the thickness of the brush $\sigma \sim d^n$ with n having the value 0.41 $\pm$ 0.07 for unannealed PS brushes and 0.32 $\pm$ 0.02 for the annealed brushes.

Acknowledgment. The authors thank Dr. Sergei F. Lyuksyutov for the use of his AFM and clean room facilities. This research was funded in part by an MURI grant (DAAH04-96-1-0018) from the Army Research Office and the Ohio Board of Regents. Use of the Advanced Photon Source was supported by the U.S. Department of Energy, Office of Science, Office of Basic Energy Science, under Contract DE-AC02-06CH11357.

References and Notes

(1) Milner, S. T. *Science* **1991**, *251*, 905.
(2) Braslau, A.; Pershan, P. S.; Swisliw, G.; Ocko, B. M.; Als Nielsen, J. *Phys. Rev. A* **1988**, *38*, 2457.
(3) Sanyal, M. K.; Sinha, S. K.; Huang, K. G.; Ocko, B. M. *Phys. Rev. Lett.* **1991**, *66*, 628.
(4) Tidswell, I. M.; Rabedeau, T. A.; Pershan, P. S.; Kosowsky, S. D. *Phys. Rev. Lett.* **1991**, *66*, 2108.
(5) Ocko, B. M.; Wu, X. Z.; Sirota, E. B.; Sinha, S. K.; Deutsch, M. *Phys. Rev. Lett.* **1994**, *72*, 242.
(6) Doerr, A. K.; Tolan, M.; Prange, W.; Schlomka, J.-P.; Seydel, T.; Press, W. *Phys. Rev. Lett.* **1999**, *83*, 3470.
(7) Tolan, M.; Seeck, O. H.; Schlomka, J.-P.; Press, W.; Wang, J.; Sinha, S. K.; Li, Z.; Rafailovich, M. H.; Sokolov, J. *Phys. Rev. Lett.* **1998**, *81*, 2731.
(8) Wang, J.; Tolan, M.; Seeck, O. H.; Sinha, S. K.; Bahr, O.; Rafailovich, M. H.; Sokolov, J. *Phys. Rev. Lett.* **1999**, *83*, 564.
(9) Tolan, M.; Seeck, O. H.; Wang, J.; Sinha, S. K.; Rafailovich, M. H.; Sokolov, J. *Physica B* **2000**, *283*, 22.
(10) Shin, K.; Pu, Y.; Rafailovich, M. H.; Sokolov, J.; Seeck, O. H.; Sinha, S. K.; Tolan, M.; Kolb, R. *Macromolecules* **2001**, *34*, 5620.
(11) Shindler, J. D.; Mol, E. A. L.; Shalaginov, A.; de Jeu, W. H. *Phys. Rev. Lett.* **1995**, *74*, 722.
(12) Mol, E. A. L.; Wong, G. C. L.; Petit, J. M.; Rieutord, F.; de Jeu, W. H. *Phys. Rev. Lett.* **1997**, *79*, 3439.
(13) Tolan, M. *X-Ray Scattering from Soft Matter Thin Films: Materials Science and Basic Research*; Springer Tracts in Modern Physics, Vol. 148; Springer: New York, 1999.
(14) Gautam, K. S.; Schwab, A. D.; Dhinojwala, A.; Zhang, D.; Dougal, S. M.; Yeganeh, M. S. *Phys. Rev. Lett.* **2000**, *85*, 3854.
(15) Lurio, L.; Kim, H.; Ruhm, A.; Basu, J.; Lal, J.; Sinha, S. K.; Mochrie, S. G. J. *Macromolecules* **2003**, *36*, 5704.
(16) Seo, Y.-S.; Koga, T.; Sokolov, J.; Rafailovich, M. H.; Tolan, M.; Sinha, S. K. *Phys. Rev. Lett.* **2005**, *94*, 157802.
(17) Guiselin, O. *Europhys. Lett.* **1992**, *17*, 225.
(18) Li, C.; Kim, H.; Jiang, J.; Li, C.; Koga, T.; Lurio, L.; Schwarz, S.; Narayanan, S.; Lee, H.; Lee, Y. J.; Jiang, Z.; Sinha, S.; Rafailovich, M. H.; Sokolov, J. C. *Europhys. Lett.* **2006**, *73*, 899.
(19) Prucker, O.; Rühe, J. *Macromolecules* **1998**, *31*, 592.
(20) Prucker, O.; Rühe, J. *Macromolecules* **1998**, *31*, 602.
(21) Prucker, O.; Rühe, J. *Langmuir* **1998**, *14*, 6893.
(22) Husseman, M.; Malmström, E. E.; McNamara, M.; Mate, M.; Mecerreyes, D.; Benoit, D. G.; Hedrick, J. L.; Mansky, P.; Huang, E.; Russell, T. P.; Hawker, C. J. *Macromolecules* **1999**, *32*, 1424.
(23) (a) Jordan, R.; Ulman, A.; Kang, J. F.; Rafailovich, M. R.; Sokolov, J. *J. Am. Chem. Soc.* **1999**, *121*, 1016. (b) Jordan, R.; Ulman, A. *J. Am. Chem. Soc.* **1998**, *120*, 243. (c) Zhao, B.; Brittain, W. J. *Macromolecules* **2000**, *33*, 342.
(24) Zhao, B.; Brittain, W. J. *Prog. Polym. Sci.* **2000**, *25*, 677.
(25) Cosgrove, T.; Ryan, K. *Langmuir* **1990**, *6*, 1361.
(26) Cosgrove, T.; Heath, T. G.; Ryan, K.; Crowley, T. L. *Macromolecules* **1987**, *20*, 1361.
(27) Parsonage, E.; Tirrell, M.; Watanebe, H.; Nuzzo, R. *Macromolecules* **1987**, *24*, 1987.
(28) Auroy, P.; Auvray, L.; Leger, L. *Phys. Rev. Lett.* **1991**, *66*, 719.
(29) Perahia, D.; Wiesler, D. G.; Satija, S.; Fetters, L. J.; Sinha, S. K.; Milner, S. T. *Phys. Rev. Lett.* **1994**, *72*, 100.
(30) Fytas, G.; Anastasiadis, S. H.; Seghrouchni, R.; Vlassopoulos, D.; Li, J. B.; Factor, B. J.; Theobald, W.; Toprakcioglu, C. *Science* **1996**, *274*, 2041.
(31) Yakubov, G. E.; Loppinet, B.; Zhang, H.; Rühe, J.; Sigel, R.; Fytas, G. *Phys. Rev. Lett.* **2004**, *92*, 115501-1.
(32) Michailidou, V. N.; Loppinet, B.; Prucker, O.; Rühe, J.; Fytas, G. *Macromolecules* **2005**, *38*, 8960.
(33) Anastasiadis, S. H.; Fytas, G.; Vlassopoulos, D.; Likhtman, A.; Semenov, A. N.; Toprakcioglu, C.; Li, J.; Factor, B.; Seghrouchni, R.; Theobald, W. *Macromol. Symp.* **1999**, *139*, 31.
(34) Fredrickson, G. H.; Ajdari, A.; Leibler, L.; Carton, J.-P. *Macromolecules* **1992**, *25*, 2882.
(35) Xi, H-W.; Milner, S. *Macromolecules* **1996**, *29*, 4772.
(36) Akgun, B.; Brittain, W. J.; Li, X.; Wang, J.; Foster, M. D. *Macromolecules* **2005**, *38*, 8614.
(37) Kim, H.; Foster, M. D.; Zhang, H.; Prucker, O.; Rühe, J.; Narayanan, S.; Wang, J. *Polymer* **2005**, *46*, 2331.
(38) *Polymer Handbook*; Brandrup, J., Immergut, E. H., Grulke, E. A., Eds.; Wiley & Sons: New York, 1999.
(39) Parratt, L. G. *Phys. Rev.* **1954**, *95*, 359. Parratt, L. G. *J. Chem. Phys.* **1956**, *53*, 597.
(40) Sinha, S. K.; Sirota, E. B.; Garoff, S.; Stanley, H. B. *Phys. Rev. B* **1988**, *38*, 2297.
(41) Yoneda, Y. *Phys. Rev.* **1963**, *131*, 2010.
(42) Lee, D. R.; Park, Y. J.; Kim, D.; Jeong, Y. H.; Lee, K.-B. *Phys. Rev. B* **1998**, *57*, 8786.
(43) Jiang, J. S.; Pearson, J. E.; Liu, Z. Y.; Kabius, B.; Trasobares, S.; Miller, D. J.; Bader, S. D.; Lee, D. R.; Haskel, D.; Srajer, G.; Liu, J. P. *Appl. Phys. Lett.* **2004**, *85*, 5293.
(44) Kim, H.; Rühm, A.; Lurio, L. B.; Basu, J. K.; Lal, J.; Lumma, D.; Mochrie, S. G. J.; Sinha, S. K. *Phys. Rev. Lett.* **2003**, *90*, 068302−1.
(45) Mochrie, S. G. J.; Lurio, L. B.; Rühm, A.; Lumma, D.; Borthwick, M.; Falus, P.; Kim, H. J.; Basu, J. K.; Lal, J.; Sinha, S. K. *Physica B* **2003**, *336*, 173.
(46) Kim, H.; Rühm, A.; Lurio, L. B.; Basu, J. K.; Lal, J.; Mochrie, S. G. J.; Sinha, S. K. *Physica B* **2003**, *336*, 211.
(47) Jäckle, J. *J. Phys.: Condens. Matter* **1998**, *10*, 7121.
(48) Persson, B. N. J.; Albohr, O.; Tartaglino, U.; Volokitin, A. I.; Tosatti, E. *J. Phys.: Condens. Matter* **2005**, *17*, R1.
(49) Palasantzas, G. *Phys. Rev. B* **1993**, *48*, 14472.
(50) Ramakrishnan, A.; Dhamodharan, R.; Rühe, J. *Macromol. Rapid Commun.* **2002**, *23*, 612.
(51) Klushin, L. I.; Skvortsov, A. M. *Macromolecules* **1992**, *25*, 3443.
(52) Barabasi, A.-L.; Stanley, H. E. *Fractal Concepts in Surfaces Growth*; Cambridge University Press: Cambridge, UK, 1995.
(53) Freitag, J. M.; Clemens, B. M. *J. Appl. Phys.* **2001**, *89*, 1101.

(54) Krim, J.; Heyvaert, I.; Haesendonck, C. V.; Bruynseraede, Y. *Phys. Rev. Lett.* **1993**, *70*, 57.
(55) Gomez-Rodriguez, J. M.; Baro, A. M.; Vazquez, L.; Salvarezza, R. C.; Vara, J. M.; Arvia, A. J. *J. Phys. Chem.* **1992**, *96*, 347.
(56) Vazquez, L.; Salvarezza, R. C.; Ocon, P.; Herrasti, P.; Vara, J. M.; Arvia, A. J. *Phys. Rev. E* **1994**, *49*, 1907.
(57) Yang, H. N.; Zhao, Y. P.; Wang, G. C.; Lu, T. M. *Phys. Rev. Lett.* **1996**, *76*, 3774.
(58) Mitchell, M. W.; Bonnel, D. A. *J. Mater. Res.* **1990**, *5*, 2244.
(59) Douketis, C.; Whang, H. Z.; Haslett, T. L.; Moskovits, M. *Phys. Rev. B* **1995**, *51*, 11022.
(60) Collins, G. W.; Letts, S. A.; Fearon, E. M.; McEachern, R. L.; Bernat, T. P. *Phys. Rev. Lett.* **1994**, *73*, 708.
(61) Zhao, Y.-P.; Fortin, J. B.; Bonvallet, G.; Wang, G.-C.; Lu, T.-M. *Phys. Rev. Lett.* **2000**, *85*, 3229.
(62) Biscarini, F.; Samori, P.; Greco, O.; Zamboni, R. *Phys. Rev. Lett.* **1997**, *78*, 2389.
(63) Kardar, M.; Parisi, G.; Zhang, Y.-C. *Phys. Rev. Lett.* **1986**, *56*, 889.

MA0708794